American Mineralogist, Volume 83, pages 228–235, 1998

Off-center hot spots: Double thermocouple determination of the thermal gradient in a 1.27 cm (1/2 in.) CaF_2 piston-cylinder furnace assembly

Jennifer M. Pickering, Brandon E. Schwab, and A. Dana Johnston

Department of Geological Sciences, University of Oregon, Eugene, Oregon 97403-1272, U.S.A.

Abstract

Double-thermocouple experiments were carried out at 10 kbar in a 1.27 cm (1/2 in.) piston-cylinder apparatus to map the thermal gradient and locate the peak temperature of a CaF_2-graphite furnace assembly over the temperature interval 900–1500 °C. An unexpected but reproducible result was that the thermal peak is displaced upward significantly (toward the steel base plug) from the vertical center of the graphite heater tubes.

The hot spot of our assembly, defined as the region no more than 10 °C cooler than the peak temperature, is displaced upward from the center of the furnace and moves slightly toward the center with increasing temperature. At a maximum temperature of 914 °C, the center of the hot spot was 2.6 mm above the mid-point of the furnace, while at 1510 °C, the highest temperature investigated, the center of the hot spot was 2.2 mm above the center of the furnace. The hot spot varies in width from 3.2 mm at lower temperatures to 2.2 mm at 1510 °C. We attribute the upward displacement of the hot spot to the greater thermal conductivity of the lower tungsten-carbide piston (k = 100W/mK at 200 °C) relative to the upper stainless steel base plug (k = 25 W/mK at 600 °C). The piston apparently conducts heat more efficiently downward than the steel plug does upward, thus displacing the hot spot upward from the furnace center.

Introduction

Steep thermal gradients are intrinsic to the design of the piston-cylinder apparatus. In most such devices, samples are enclosed in an approximately 3–4 cm long, 1.27 cm (1/2 in.) or 1.91 cm (3/4 in.) diameter furnace assembly that is then placed inside the axial hole of the pressure vessel. This vessel (or bomb plate as it is known in many labs) is typically about 5 cm thick and is cooled along the top and bottom surfaces with flowing water. In many configurations, a sheet of mylar lies between the cooling water and the top of the vessel. Heat is generated within the furnace assembly by running an electrical current through a thin-walled graphite tube, which heats resistively. As the graphite furnace tube is the only assembly part that generates significant heat, the thermal gradient along the vertical axis of the full assembly is greatest within the portion spanned by the graphite furnace. Previous studies in talc assemblies (Boyd and England 1960, 1963; Cohen et al. 1967) suggested that the gradient is symmetrical with respect to the furnace center. Recent studies of NaCl-Pyrex assemblies (Hudon et al. 1994; Dunn 1993) also infer a hot spot centered within the furnace. However, with the exception of Hudon et al. (1994), these studies do not address the effect of compression during experiments on the position of the thermocouples. In particular, it is unclear whether reported thermocouple positions are measured pre- or post-experiment, leaving the data ambiguous to interpret. Nevertheless, as a result of these findings, most piston-cylinder laboratories center the sample capsule within the furnace tube of their particular assembly. We show that assuming that the peak temperature is centered vertically in the furnace is not always valid and can have undesirable consequences if large sample capsules are used.

During an experiment, the crimped and folded capsules are positioned very close to the thermocouple with their narrow dimensions oriented vertically. These capsules probably do not experience large thermal gradients simply because their smaller dimensions are aligned parallel to the long axis of the furnace. In addition, at the lower temperatures where gold capsules are often used, thermal gradients are less steep and the hot spot region is larger (Boyd and England 1963, Fig. 1; Hudon et al. 1994). However, when graphite liners are used to isolate samples from outer platinum capsules, significantly larger capsules must be used to accommodate both the liner and sample volume. Graphite-lined platinum sample capsules used in this study, initially 4 to 4.5 mm in length, compress to 2.8 to 3.2 mm during experiments. If not placed correctly within the hot spot, such large capsules can experience large thermal gradients, especially when carried out at the high temperatures necessary in peridotite melting experiments (>1200 °C).

In Figure 1 we show spinel compositions from experiment FER-A-6 carried out at 1280 °C for 96 h. The disconcerting variability of these data motivated this study. With increasing temperature and concomitant increase in partial melting, the $Mg/(Mg + Fe_T)$ of spinel decreases

0003–004X/98/0304–0228$05.00

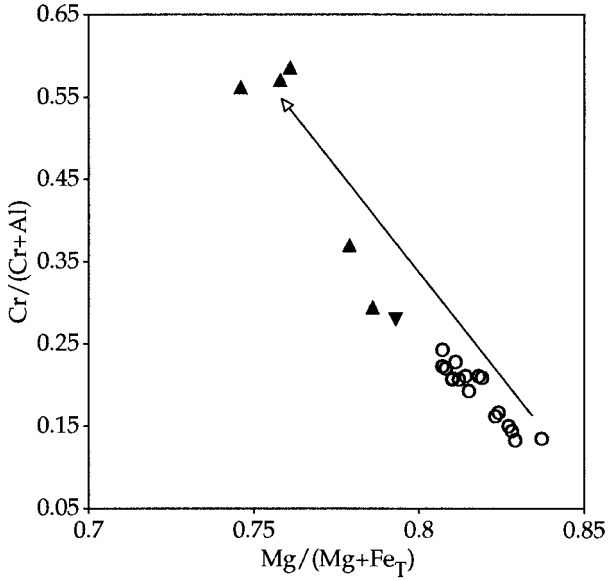

FIGURE 1. A plot of atomic Cr/(Cr + Al) vs. Mg/(Mg + Fe_T) of spinel from 10 kbar melting experiments on Kilbourne Hole xenolith [mode = Olivine (50%), Opx (30%), Cpx (17%), Spinel (3%)]. Filled triangles are mean spinel compositions from the melting experiments of Baker and Stolper (1994) from 1270 to 1390 °C. Open circles are multiple spinel analyses from FER-A-6, our 1280 °C experimental product. Designed specifically to replicate their 1280 °C/10 kbar experiment (indicated by the inverted triangle), our 1280 °C experiment utilized identical starting material to that used by Baker and Stolper (1994). The arrow indicates the trend of changing spinel compositions with increasing temperature and extent of partial melting.

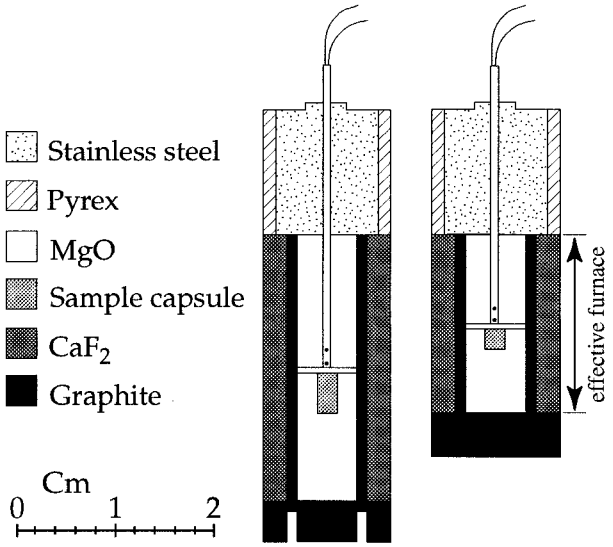

FIGURE 2. Cross section of pre- and post-experiment 1.27 cm (1/2 in.) furnace assemblies. Drawn to scale, the illustration at right is typical of the average 30% overall shortening we see in our experiments carried out at 10 kbar. Note the compaction of the lower graphite parts to accommmodate furnace extrusion, which is discussed in the text.

and the Cr/(Cr + Al) increases, as indicated by the arrow in Figure 1. Thus the trend spanned by the spinel analyses from our single 1280 °C experiment product (open circles) suggests that a large thermal gradient was present across the sample capsule and possibly that the sample temperature was <1280 °C at all points along the length of the capsule. Dissecting experiment FER-A-6 after quench confirmed that the sample capsule was centered in the furnace during the experiment, and that the thermocouple had indented the top of the capsule. Hence, we infer that the spatial variation in spinel composition within the experimental product depicted in Figure 1 resulted from a significant thermal gradient across the 3 mm vertical dimension of the sample capsule. This deduction leads to the conclusion that sample FER-A-6 was not centered on the hot spot, and therefore the hot spot is not centered within the furnace in our assembly. To determine where the hot spot is in our CaF_2-graphite assembly, we carried out the double-thermocouple experiments discussed in the remainder of this paper.

THE ASSEMBLY

Experiments were conducted using a cell with an outer CaF_2 sleeve, a straight-walled graphite furnace, and two inner pieces of crushable MgO (Fig. 2). The upper MgO piece had an axial hole for the thermocouple, and a dummy sample, contained in a graphite-lined platinum capsule, was set into a cavity drilled into the solid lower piece of MgO and surrounded by MgO powder. A thin (0.5 mm) wafer of MgO separated the end of the thermocouple from the top of the sample capsule. In all but one experiment, the length of the upper MgO piece equaled the combined length of the lower MgO piece plus the thin wafer. In one experiment conducted without a sample capsule, the upper MgO piece with the axial hole for the thermocouple was cut a little longer than half the length of the furnace, to allow measurement of the thermal gradient below the furnace center.

Our assembly, modified after that used by Boettcher et al. (1981), incorporates a graphite ring and plug at the base of the assembly, which provides a small empty space into which the furnace slides during compression (Fig. 2). To ensure that the furnace seats properly in this space, furnace tubes are cut 1 mm longer than the combined inner MgO parts. This configuration results in unsheared, uniformly compressed furnaces, which contribute to power stability during experiments. Before inserting the assemblies into the pressure vessel, they are wrapped in 0.7 mm thick lead foil, and the inner wall of the carbide core is coated with a thin layer of MoS_2 lubricant.

EXPERIMENTAL PROCEDURE

Temperatures were measured using W_5-Re/W_{26}-Re thermocouple (tc) wires calibrated by Englehard Industries. Calibrations are traceable to National Bureau of Standards tests nos. 243484A and 233064E, with estimated uncertainties not exceeding 0.4% of the tempera-

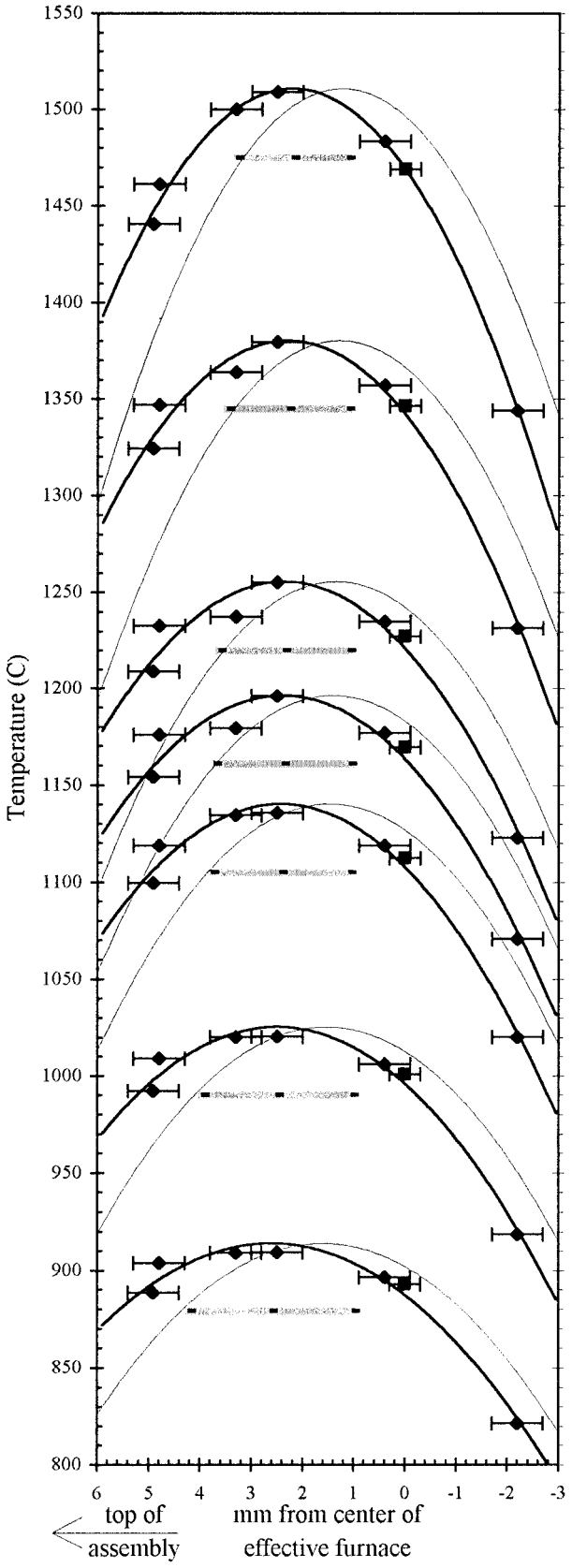

FIGURE 3. The results of six double-thermocouple experiments are plotted as temperature (°C) vs. distance (mm) from the center of the post-experiment effective furnace. Each thick curve represents a second-order polynomial fit to all six experiments at a given mV step for the centered control tc. Each individual experiment is represented by the control tc in the center and one point offset above or below 0 mm on each curve. Errors in temperature measurements are less than the vertical dimension of the symbols. The ±0.5 mm distance error bars represent a combination of the authors' ability to reproduce independently a given measurement of the post-experiment assembly (±0.2 mm) and the allowed ±0.3 mm variance on the control thermocouple being out-of-center (see text). The bars below each curve represent the width of the 10 °C hot spot for that curve. The tick mark in the center of each bar represents the position of the peak temperature. The thin curves are calculated model gradients, discussed in the text.
←

ture in the range investigated. All tc voltages were measured without cold junction compensation, and no pressure corrections were applied to the emf of the thermocouples. To compensate for the cold junction of the thermocouples being at room temperature rather than 0 °C, a value of 0.2 mV was added to every emf measurement taken. Second-order polynomial regressions of temperature vs. the calibrated mV values provided by Engelhard allowed quantitative calculations of the temperatures corresponding to the emf readings.

Four-bore mullite insulators housed the thermocouple wires. Two thermocouples were welded into a single tube by grinding away one side of the four-bore tubing to expose two of the holes a few millimeters from the end, then inserting two sets of wires and spot welding under argon gas, one pair at each exposure. This procedure resulted in small shiny beads that did not protrude outside the outer diameter of the mullite tubing. During all experiments, a Eurotherm 808 digital temperature controller maintained the temperature of the thermocouple located in the center of the furnace. Temperatures at incremental distances above or below the central control thermocouple were measured passively with the second thermocouple, using a digital multimeter.

Experiments were maintained at 10 kbar ±83 bars. Reported pressures are nominal Heise gauge pressures, with no friction correction. Experiments were pressurized at room temperature to approximately 9.5 kbar, heated to an emf of 21.0 mV (1164 °C, after applying the cold junction compensation), and allowed to equilibrate thermally. In every case, thermal expansion resulted in the final pressure adjustment to 10 kbar being a pressure release (i.e., hot piston-out). The emf of the control thermocouple was then increased in 1.0 mV increments at a ramping rate of 1.5 mV/min, to a maximum of 26.0 mV (1469 °C). Temperature was then ramped downward in 2.0 mV increments to 16.0 mV (893 °C), and the emf of the passive tc was recorded 90 s after reaching each target temperature. This procedure was repeated once more, ramping

temperature back up to 26.0 mV, then down to 16.0 mV, and recording the emf of the passive tc at each temperature step. A time interval of 90 s was sufficient for the emf outputs of both thermocouples to stabilize. This was tested by taking a measurement after 90 s, then monitoring the values over a 30 min period, over which the emf of the passive tc fluctuated no more than ± 0.03 mV. The emf measured at each temperature step during upward rampings varied no more than ± 0.10 mV from the emf measured at the same step during downward rampings. The emf measurements reported in Figure 3 were all recorded on the first downward ramp of each experiment.

Discussion of the effects of compression

After a 10 kbar experiment, we typically observe 30% shortening of our CaF_2-graphite assembly. We believe that the shortening is due primarily to our inability to manufacture CaF_2 parts with densities greater than about 85% of the density of single-crystal fluorite using our bench press and die. As we pressurize our assemblies, the CaF_2 further compacts as the furnace tube slides into the space provided by the graphite ring and plug at the assembly bottom. When starting an experiment, we pump the master ram to within 0.5 kbar of the target pressure, then begin ramping up to the target temperature. During temperature ramping, the master ram pressure typically falls due to compaction of the assembly, requiring continuous pumping to maintain the sample pressure near the desired value. When the target temperature is reached, or soon after, thermal expansion of the assembly results in master ram pressure increasing, requiring a pressure release to maintain the target pressure until thermal equilibrium is achieved. Thus it appears that the shortening of the assembly occurs almost entirely during the temperature ramping to the desired set point and that the effective geometry during the experiment is that of the compressed assembly.

We carefully monitored the effects that compression of the assembly during the experiment had on the results, which were twofold. First, compaction of the thermocouple welds into the mullite tubing resulted in the welds being approximately 1 mm closer together after each experiment, regardless of how far separated they were before compression. Second, differential compression of the inner MgO parts may result in the control thermocouple moving to an out-of-center position during the experiment. To compare results from one experiment to another, the control thermocouple must always be located in the same place within the assembly. If the control thermocouple was >0.3 mm away from center, the experiment was discarded and repeated. Furthermore, furnace extrusion into the empty space provided by the basal graphite ring and plug during initial compression allows the inner MgO parts to compress more than the furnace. The shortening of the inner MgO parts draws the previously mentioned small graphite plug into the furnace (Fig. 2). Thus the length over which the furnace is actually thin-walled is equivalent to the combined length of the shortened inner MgO parts. We consider this length the effective furnace, and believe that it is along this length that heat is generated, rather than the length of the pre-experiment furnace. Henceforth, we refer to the post-experiment length of the inner MgO parts as the effective furnace and the full length of the graphite tube as the full furnace.

To get an accurate profile of the thermal gradient in an assembly during an experiment, we dissected all charges post-experiment and carefully measured the length of the effective furnace, the position of the control thermocouple, and the distance separating the two thermocouples during the experiment with a digital micrometer. Hence the distance of the passive thermocouple (in millimeters) from the center reported in Figure 3 represents the position of the passive thermocouple, relative to the center of the compressed effective furnace, during the actual conditions of the experiment. Neglecting the effects of compression on double-thermocouple determinations of thermal gradients results in broader curves and ambiguous peak temperature positions with respect to the center of the furnace. Such inaccuracies lead to underestimates of the thermal slope of the gradient and hence overestimates of the length of the hot spot and possibly lead to an erroneous placement of the sample in the assembly with respect to the thermal peak.

Results

In contrast to previous studies (e.g., Boyd and England 1960, 1963; Cohen et al. 1967; Dunn 1993), the thermal peak in the assembly described here is not located in the center of the effective furnace, but is displaced upward toward the steel base plug by approximately 2.5 mm. Figure 3 shows the vertical thermal gradients measured over a 7 mm span from just below the center of the effective furnace upward toward the base plug. The thermal gradient was measured at 10 kbar over the temperature interval 900–1500 °C.

With increasing temperature, the location of the thermal peak moves toward the center of the effective furnace (Fig. 3). In the lowest temperature experiment reported, a peak temperature of 914 °C was located 2.6 mm above the center of the effective furnace, whereas at 1510 °C the peak had moved to within 2.2 mm of the center. For each experiment we calculated the length of the zone within which the temperature was no cooler than 10 °C below the peak temperature, which we consider as an acceptable hot spot. This hot spot zone was 3.2 mm in length at lower temperatures, decreasing to $\sim$2.7 mm for temperatures in the range 1000–1300 °C. Above 1300 °C, the hot spot zone shortened to 2.4 mm and was only 2.16 mm long at 1510 °C. This shortening of the hot spot results from the steepening of the thermal gradient with increasing temperature, as has been observed in other studies (e.g., Boyd and England 1963; Hudon et al. 1994).

A displacement of the hot spot approximately 1–2 mm upward toward the base plug also has been observed in NaCl and NaCl-Pyrex assemblies having configurations almost identical to that shown in Figure 2 (T.C. McCar-

thy, personal communication, 1997). Although all three assemblies started with a pre-experiment full furnace length of 27.5 mm, the NaCl-Pyrex and NaCl assemblies shortened considerably less during experiments because NaCl powder can be pressed to nearly the density of single-crystal halite using a bench press (post-experiment full furnace lengths averaged 22.5 mm in NaCl-Pyrex and 24.8 mm in NaCl, compared with 20 mm in our experiments in CaF_2). It thus appears that off-center hot spots may occur even in assemblies with longer furnaces. However, effective furnace lengths were not measured post-experiment in the NaCl and NaCl-Pyrex assemblies, precluding a rigorous comparison of the results of the two studies.

Thermal model

In collaboration with Michael Manga at the University of Oregon, we simplified the assembly into a one-dimensional (parallel to the axis of symmetry) model in an attempt to understand the cause of the upward shift of the thermal peak of our assembly relative to the midpoint of the effective furnace. The symmetry of the assembly and pressure vessel about the vertical axis implies that heat flow in the radial direction is symmetric. Thus we assume that heat flow in the radial direction does not contribute to displacements of the thermal peak up or down along the vertical axis of the assembly.

As shown in Figure 4a, the model consists of three layers of different thickness. Layer one, 12 mm thick, represents the steel base plug, and layer two, 18 mm thick, represents the effective furnace. These layers have thermal conductivities k and k', respectively. The third layer, representing the lower graphite parts and the portion of the tungsten-carbide (WC) piston within the pressure vessel during a typical experiment with our assembly, is 20 mm thick and has a different conductivity, k''. The furnace layer (the middle layer) has constant heat production, A. Heat production is zero in the base plug layer and in the graphite plug + WC-piston layer. Using the boundary conditions that $T = 0$ at the top and bottom of the model, and that heat flux and T are continuous across the boundaries between layers, one can solve the steady-state heat flow equation:

$$k\frac{d^2T}{dx^2} = -A \tag{1}$$

for the temperature distribution in the axial (x) direction.

Despite its simplicity, the model offers a physical explanation for the observed displacement of our hot spot toward the material with low thermal conductivity, the steel base plug. To illustrate this hypothesis, we show a few generic calculations in Figure 4b. We begin by investigating the effect of varying the ratio between the conductivities of the steel plug and the WC-piston. For simplicity in these calculations, we consider the conductivity of both the base plug and furnace layers to be the same ($k = k'$), and we vary the conductivity of the WC-piston layer (k'') from this value to higher values. We first solve the case where conductivity in all three layers is the same. This gives a curve (Fig. 4b) with a peak temperature located 1.4 mm below the center of the middle layer (the furnace), reflecting the fact that the layer representing the portion of the piston within the vessel is thicker than that representing the steel base plug. As the conductivity ratio (k/k'') between the combined base plug and furnace layers and the piston layer decreases, the peak temperature is displaced away from the piston, which is the material with higher conductivity. At a conductivity ratio $k/k'' = 0.6$, the peak temperature is centered in the furnace layer. As k/k'' continues to decrease, the peak temperature continues to migrate toward the steel plug, as observed in our assembly. The position of the peak temperature relative to the center of the furnace layer is plotted in Figure 4c as a function of the conductivity ratio k/k'' for an assembly with the same dimensions as ours.

To model our specific assembly, we need estimates of the actual thermal conductivities of the three model layers. For the thermal conductivity of the base plug and WC-piston layers, we use values of 25 W/mK (AISI stainless steel 304 at 600 °C, Bejan 1983) and 100 W/mK (at 200 °C, Carboloy, product information, 1997), respectively. We assume these values are valid to elevated temperatures as both materials are metals without a strong dependence of conductivity with temperature (Berman 1976). To estimate a bulk thermal conductivity for the middle layer, which consists of a graphite furnace tube surrounded by CaF_2 and filled with MgO, we used the method given in Kingery (1960) for calculating thermal conductivity of multiphase bodies. We assume the concentric cylinders of materials in our assembly behave as a series of slabs, with heat flow parallel to the plane of the slabs. For the bulk thermal conductivity of this geometry, Kingery (1960) gives the equation $k' = \Sigma V_i k_i$ where V_i is the volume fraction (cross-sectional area) of each component, and k_i is the thermal conductivity of that component.

At temperatures above 727 °C, k of CaF_2 approaches an approximately constant value of 2.3 W/mK (Touloukian 1967). The thermal conductivity of MgO decreases with increasing T, ranging from ~54 W/mK at 0 °C to ~7.5 W/mK at 1500 °C (Touloukian 1967). However, in the temperature range of this study between 900 and 1500 °C, k of MgO varies only from ~5.4 W/mK to ~7.5 W/mK (Touloukian 1967). As MgO comprises only a quarter of the cross-sectional area of the furnace layer, and the conductivity values for MgO are relatively low, this range in conductivity results in the bulk conductivity estimate varying only ± 0.5 W/mK. Therefore, we have chosen to do our calculations with an average value of 6.45 W/mK for the conductivity of MgO. Including the temperature dependence of k of MgO would likely cause the temperature distribution curve to be slightly steeper and tighter than shown (e.g., Li et al. 1996). We assume this effect would be roughly symmetrical about the peak,

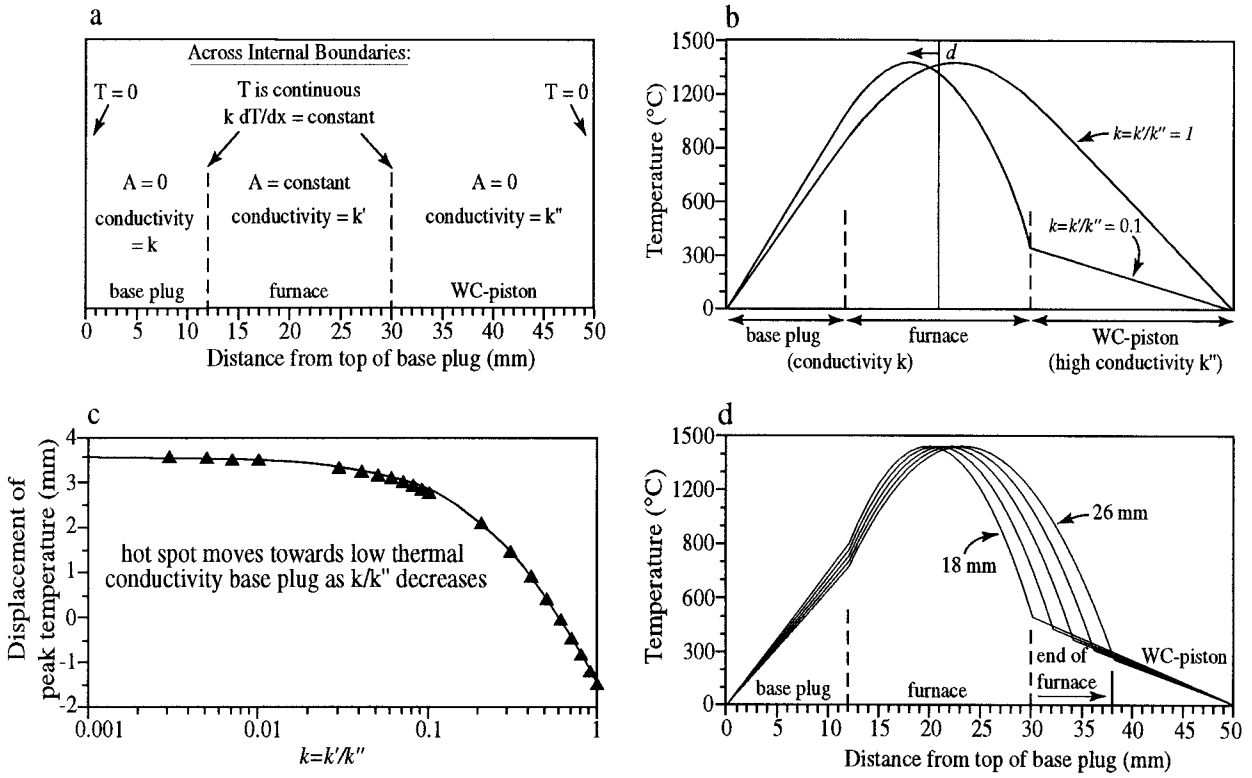

FIGURE 4. **(a)** The geometry and boundary conditions for the integration of Equation 1. **(b)** Two curves generated by integrating Equation 1. The symmetrical curve is for the simple case where $k = k'/k'' = 1$. The second curve illustrates the thermal gradient when the $k = k'/k''$ ratio is 0.1, with the 2.8 mm upward offset of the thermal peak indicated with the arrow labeled *d*. The solid vertical line represents the middle of the post-experiment effective furnace. **(c)** Displacement of the peak temperature from the center of the effective furnace plotted as a function of conductivity ratio, $k = k'/k''$. Curve shown is a second degree polynomial fit to the data: $f(x) = 2.588x^2 - 7.558x + 3.570$. **(d)** Several calculated curves illustrating the effect of lengthening the furnace. All five curves are calculated using the same conductivities as for the highest temperature (~1510 °C) model curve shown in Figure 3 ($k/k'/k'' = 25:13.3:100$). The effective furnace length was increased in 2 mm increments from 18 mm to a maximum length of 26 mm. (For clarity, only the 18 mm and 26 mm furnace length calculations are labeled.) As the furnace lengthens, the bottom end of the furnace moves from 30 mm (from the top of the base plug) to a maximum of 38 mm, as indicated by the arrow. For each calculation, the middle of the effective furnace moves away from the base plug faster than the calculated thermal peak, leaving the peak temperature displaced above the effective furnace center by increasing amounts with increasing effective furnace lengths. In order of increasing effective furnace length, calculated displacements upward from center of the thermal peak in mm are 1.2 (18 mm effective furnace), 1.4, 1.5, 1.7, and 1.8.

affecting the shape of the temperature distribution curve, but not greatly affecting the position of the thermal peak.

The thermal conductivity of graphite has a strong dependence on temperature, so a single average value does not suffice to cover the temperature range of this study. However, including the temperature dependence of *k* of graphite makes the model equation non-linear, thus greatly complicating the solution. For simplicity, we estimate the conductivity of graphite at seven 100 °C temperature steps from 900 to 1500 °C, roughly corresponding to the peak temperatures of the measured gradients shown in Figure 3. Clark (1966) provides conductivity values in the temperature range from 0 to 2500 °C for Acheson graphite, which has a conductivity of 167 W/mK at room temperature. Similar to Acheson graphite, the high-density graphite comprising our furnaces has a conductivity of 196 W/mK at room temperature (Carbone, product information, 1997). To estimate the conductivity of our graphite at higher temperatures, we applied the temperature dependence of Acheson graphite and extrapolated from the value of 196 W/mK at room temperature to higher temperatures. A second-order polynomial regression of the data projected in this fashion allowed us to estimate the thermal conductivity of the graphite used in our furnaces in 100 °C steps from 900 to 1500 °C. We use these estimated values for *k* of graphite (in order of increasing temperature in W/mK: 91.0, 83.1, 75.8, 69.3, 63.3, 58.1, and 53.5) in conjunction with the *k* values of 2.3 W/mK for CaF_2 and 6.45 W/mK for MgO to calculate a bulk conductivity for the furnace layer at the seven temperature steps. The resultant estimates for the bulk conductivity of the furnace layer (from 900 to 1500 °C,

in W/mK: 20.5, 19.0, 17.6, 16.3, 15.2, 14.2, and 13.3) were then used to calculate the seven model curves shown in Figure 3. Note however that this procedure does not account for the fact that temperature, and thus the thermal conductivity of graphite, vary along the length of the furnace at any particular peak temperature.

The solutions specific to our assembly parameters are plotted as thin lines on each gradient shown in Figure 3. At the lowest temperature investigated, the model predicts a displacement of the 914 °C peak 1.6 mm upward from the center of the effective furnace, compared with the measured offset of 2.6 mm above center. With increasing temperature, the offset of the thermal peak in both the model and measured gradients decreases. At the highest temperature investigated, the model predicts a displacement of the 1510 °C peak 1.2 mm above the effective furnace center, compared with the measured offset of 2.2 mm above center. The approximations and inherent uncertainties in the model warrant caution in applying its predictive power, but the relatively good agreement between the measured and predicted gradients suggests the model captures the essence of the problem.

It is important to note that all of the modeling results presented above pertain to assemblies with dimensions and materials like those used in our lab. We are aware that several labs use furnace assemblies that are significantly longer than ours. Consequently, we have thus investigated the effect of lengthening the furnace layer of the overall assembly, leaving everything else the same as for the 1510 °C model curve ($k{:}k'{:}k''$ = 25:13.3:100). Figure 4d shows the result of this exercise when the length of the post-experiment effective furnace is increased in 2 mm increments from 18 to 26 mm. As expected, the position of the thermal peak moves away from the base plug with increasing furnace length. However, as the furnace lengthens, the center of the furnace moves away from the base plug faster than the thermal peak, leaving the thermal peak displaced upward by increasing amounts. Thus the calculations suggest longer furnaces do not lessen the hot spot displacement. As other labs that use longer furnaces than ours have not reported offset hot spots, this result may indicate that the simplifying assumptions have compromised the accuracy of the model. Heat flow in the radial direction or the effect of temperature dependence on thermal conductivities may have a greater effect on the position of the thermal peak than we have assumed. However, the fact that the model curves calculated using the parameters specific to our assembly are in relatively good agreement with our measured gradients (Fig. 3) leaves us no cause to dispute the suggestion that longer furnaces may also have offset hot spots. We cannot provide further empirical evidence either supporting or casting doubt on this suggestion, as we did not measure the thermal gradient in a furnace with a post-experiment length longer than 18 mm. We stress that our principal aim with this contribution is to present the measured gradients, documenting an offset hot spot in our assembly. We present the model merely to illustrate the effect that differences in the conductivities of materials in the axial direction may have on the location of the thermal peak. Primarily based on these measurements, and in part the model results, we recommend that other labs measure the thermal gradient in their own assemblies, making allowances for any effects assembly compression might have.

Conclusions

As the assembly and pressure vessel are symmetrical in the radial direction, the variation in thermal parameters of materials in the axial direction has the greatest effect on the position of the thermal gradient along axis. Of these, our results suggest that the most significant factors are the thermal conductivity ratio between the steel plug and WC-piston and the length of the furnace. Shortening the steel plug reduces the upward displacement of the thermal peak. The results of our simplified model do not corroborate the general assumption that longer furnaces may cause the peak temperature to move closer to the effective furnace center. Further work on determining the thermal gradients in assemblies with effective furnaces longer than 18 mm is required to resolve the effect of furnace length on the location of the thermal peak along the axis of the assembly. Regardless of the effect on the position of the thermal peak, longer furnaces result in a wider hot spot zone, making it easier to place a capsule entirely within the hot spot. By decreasing the gradient in the center of the furnace, stepped or tapered furnaces (e.g., Kushiro 1976) would likely dampen the effect of hot spot displacement on the thermal gradient experienced by a sample centered within the furnace. However, stepped or tapered furnaces introduce additional challenges with their construction and may not be time or cost effective for many labs.

As a result of the observations reported here, we have relocated the sample-thermocouple interface in our experiments to 3.5 mm above the center of the furnace. This relocation places the thermal peak within the sample volume, and also places the thermocouple and capsule bottom at the edges of the hot spot, ensuring that every point within the sample is within 10 °C of the temperature measured by the thermocouple. To confirm that sample capsules and thermocouples were positioned properly with respect to the thermal gradient during experiments, we carefully dissect all charges and measure the lengths of all assembly parts post-compression. This procedure has eliminated data scatter such as that shown in Figure 1 and results in texturally and compositionally homogeneous experimental products, even when relatively large graphite-lined platinum capsules are used.

Acknowledgments

We gratefully acknowledge Michael Manga for assistance with the thermal model, Dave Senkovich and Cliff Dax for technical assistance in the Machine Shops at the University of Oregon, and T.C. McCarthy for helpful reviews of the manuscript and providing supporting data. We thank Michael Baker and John Ayers for careful reviews of the manuscript. This work was supported by NSF grant EAR-9506045.

REFERENCES CITED

Baker, M.B. and Stolper, E.M. (1994) Determining the composition of high-pressure mantle melts using diamond aggregates. Geochimica et Cosmochimica Acta, 58, 2811–2827.

Bejan, A. (1993) Heat transfer, 675 p. Wiley, New York.

Berman, B.R. (1976) Thermal conduction in solids, 193 p. Oxford University Press, New York.

Boettcher, A.L., Windom, K.E., Bohlen, S.R., and Luth, R.S. (1981) Low-friction, anhydrous, low- to high-temperature furnace sample assembly for piston-cylinder apparatus. Reviews in Scientific Instrumentation, 52, 1903–1904.

Boyd, F.R. and England, J.L. (1960) Apparatus for phase-equilibrium measurements at pressures up to 50 kilobars and temperatures up to 1750°C. Journal of Geophysical Research, 65, 741–748.

———(1963) Effect of pressure on the melting of diopside, $CaMgSi_2O_6$, and albite, $NaAlSi_3O_8$, in the range up to 50 kilobars. Journal of Geophysical Research, 68, 311–323.

Clark, S.P., Ed. (1966) Handbook of physical constants, Memoir 97, 587 p. Geological Society of America, New York.

Cohen, L.H., Ito, K., and Kennedy, G.C. (1967) Melting and phase relations in an anhydrous basalt to 40 kilobars. American Journal of Science, 265, 475–518.

Dunn, T. (1993) The piston-cylinder apparatus. In R.W. Luth, Ed., Experiments at high pressure and applications to the Earth's mantle. Mineralogical Association of Canada Short Course Handbook, 21, 39–94.

Hudon, P., Baker, D.R., and Toft, P.B. (1994) A high-temperature assembly for 1.91-cm (3/4-in.) piston-cylinder apparatus. American Mineralogist, 79, 145–147.

Kingery, W.D. (1960) Introduction to ceramics, 781 p. Wiley, New York.

Kushiro, I. (1976) Changes in viscosity and structure of melt of $NaAlSi_2O_6$ composition at high pressures. Journal of Geophysical Research, 81, 6347–6350.

Li, X., Manga, M., Nguyen, J.H., and Jeanloz, R. (1996) Temperature distribution in the laser-heated diamond cell with external heating, and implications for the thermal conductivity of perovskite. Geophysical Research Letters, 23, 3775–3778.

Touloukian, Y.S., Ed. (1967) Thermophysical properties of high temperature solid materials, thermophysical properties research center, Purdue University, vols. 1–6. MacMillan, New York.

MANUSCRIPT RECEIVED APRIL 24, 1997
MANUSCRIPT ACCEPTED NOVEMBER 1, 1997